Title–Morphological study of electrodeposited copper under the influence of ultrasound and low temperature

Authors–A. Mallik and B.C. Ray

Journal: Thin Solid Flims (2009)

Author affiliations – Rourkela Steel Plant, SAIL, Rourkela – 769011, and Dept. of Metallurgical and Materials Engg., National Institute of Technology, Rourkela – 769006, India

Address of corresponding author–

A. Mallik

Management Trainee Technical,

Rourkela Steel Plant, SAIL, India

Rourkela – 769011

Phone – 91-9778402225(O)

E-mail – archananitrkl@gmail.com

Morphological study of electrodeposited copper under the influence of ultrasound and low temperature

A. Mallik* and B.C. Ray**
*Rourkela Steel Plant, Steel Authority of India Ltd., Rourkela - 769011
**Dept. of Metallurgical and Materials Engg., National Institute of Technology, Rourkela – 769006, India
archananitrkl@gmail.com (Corresponding author, A. Mallik)

Abstract - The effects of temperature and cavitation on the electrochemistry principle were experimented here by adding the impact of sonication to synthesize ultrafine grained deposits at low temperatures. The X-ray diffraction analysis and microscopic studies confirmed the nanorange deposit. Scanning electron microscopy images have also confirmed the powdery and highly scattered deposits in silent conditions. Ultrasound was found to have a significant effect on the deposit morphology. The deposit obtained was compact, uniform and adherent. Energy dispersive spectroscopy result of the deposits revealed an oxidized silent deposit along with some adsorbed sulfur onto the electrode surface. In contrary the in-situ cleaning associated with sonication has resulted in cleaner deposits.

Keywords – Electrodeposit, Ultrasound, Temperature, Copper

1. Introduction

Electrodeposition is mostly used to obtain metallic films of adequate thickness, structure and adhesion. The high selectivity of the deposition processes allows uniform modification of surfaces and structures with complex profiles [1]. Accordingly, the effects of plating baths, plating modes, conditions as well as the effect of post-treatment on the textural characteristics of metal deposits are worthy of being studied [2,3]. Copper electrodeposition has been widely used in electronic industry for manufacturing of printed-circuit boards, interconnects, multilayer sandwiches of giant magnetoresistive hard disc read heads, protective and decorative coatings.

Electrochemical nucleation and growth are complex phenomena. The formation of deposit is dependant on time and flux. Fast mass transport causes the formation of many nucleation sites and the high flux contributes to the growth phase of the deposit [4]. Thermodynamics and kinetics of the process may depend on a number of factors. Existence of an energy barrier makes nucleation a probability process [5,6], with a rate

$$J_0 = Z_0 W \lambda^{-1} \exp\left[\frac{-\Delta G(n_c)}{kT}\right] \qquad (1)$$

Where, Z_0 /cm^{-2}is the number density of active sites on the substrate, W /s^{-1} is the frequency of attachment of single atoms to the nucleus and λ^{-1} is a non-dimensional quantity accounting for the difference between the quasi-equilibrium and the stationary number of nuclei, $\Delta G(n_c)$ is the maximum energy barrier at a critical cluster size n_c, k and T have their usual meanings. The energy barrier that the ions have to surmount for an adatom formation is

an obvious function of temperature. Decreasing temperature increases the level of supersaturation. Hence, the activity of ions will increase and the critical nucleating condition will occur at low temperature. The relationship between morphology and degree of supersaturation is an open area of research. However supersaturation determines the degree of metastability in the parent phase. To relate the non-equilibrium cluster energetic and fluctuational growth to the rate of nucleation, it is necessary to describe the cluster population distribution. The metastable equilibrium concentration of critical clusters of a given size, C_n, is then [7]

$$C_n = C_l \exp\left[\frac{-\Delta G(n)}{kT}\right] \qquad (2)$$

Where, C_l is the number of atoms per unit volume in the liquid. Thus a high nucleation rate can be achieved at low temperature.

The growth of clusters past the critical size can be represented kinetically [5,6] as:

$$J = \nu_{SL} S_{cr} C_n = \nu \exp\left(\frac{-\Delta H_d}{kT}\right) S_{cr} C_l \exp\left[\frac{-\Delta G(n)}{kT}\right] \qquad (3)$$

Where, ν_{SL} is the jump frequency of atoms form the liquid to the critical cluster (It can be estimated from lattice vibration frequency ν and activation energy barrier for interfacial diffusion ΔH_d), S_{cr} is the number of atoms surrounding a cluster and C_n is the number of critical clusters. At low temperature**,** the population of critical clusters increases whereas the rate of attachment of further atoms to the cluster decreases due to increased diffusion barrier.

Hence temperature can affect the crystal growth by several ways, all of them predominantly resulting in a smaller crystal size at low temperatures [8,9].

Acoustic cavitation is the phenomena of sequential formation, growth and collapse of microscopic bubbles (voids) in the liquid [10,11] in presence of an ultrasonic field. This sequence can produce temperatures as high as those on surface of the sun and pressure as great as those in the bottom of the ocean. Thus cavitation, by concentrating the diffused fluid locally in a very short duration creates a zone of intense energy dissipation. The sequential cavitation phenomena will thus create an extremely high level of localized supersaturation, resulting in triggered nucleation [12]. It has been proposed by various investigators that cavitation of electrolyte by acoustic streaming causes fast mass transport [13,14,15], degassing [16,17] and in situ cleaning [15,18] at the electrode surface. An extensive review on the versatile use of ultrasound in an electrochemical context has been given by C. E. Bank and R. G. Compton [19]. Ultrasound is also capable of inducing crystal breakage. This may further enhance the nucleation process by secondary nucleation. Remarkable increase in mass transport, the most distinct effect of cavitation, enables it to modify a diffusion controlled system to a charge transfer system [20,21]. Contribution of cavitation, thus, should affect nucleation more rather than growth. However increase in mass transport may also possibly affect grain growth. Hence the dominance of opposing effects of sonication and thermal environment are more likely to be contradictory and far from conclusion.

The above mentioned effects of temperature and cavitation on the electrochemical crystallization principle are investigated in the present study. Electrochemical nucleation and growth phenomena are mainly quantified by electroanalytical measurements like

potentiometry, voltammetry, polarography, coulometry and chronoamperometry. The present experiment aims here to prove the conventional hypothesis by different microscopic techniques and X-ray diffraction (XRD) method.

2. Experimental details

Copper was potentiostatically deposited from a simple aqueous solution of $CuSO_4$ (10 g l^{-1}) and H_2SO_4 (40 g l^{-1}) in an open cell. Double distilled water and analytical grade chemicals were used. Saturated calomel electrode was used as the reference electrode. Electrodeposition was done in a fixed over potential range of 100 mV to 600 mV at a sweep rate of 1 mV/s onto rough graphite electrodes from a pure copper anode. Temperature ranges selected for the above experimentation are 25 ˚C, 19.5 ˚C, −1 ˚C and −3 ˚C. A freezer was used to maintain low temperature conditions. Experiments were performed in absence of antifreezers to avoid/minimize convoluting complications by the presence of foreign particles. An ultrasonic cleaner of 30 kHz frequency, with 60 watts power with an inbuilt thermostatic heater of 0.04 kW was used for sonication impact.

Several techniques have been used to characterize the deposits. XRD patterns were recorded from 30˚ to 140˚ with a Philips X-pert MPD system diffractometer using Cu K_α at an accelerating voltage of 40 kV. Data was collected at a counting rate of 1˚/min. The K_α doublets were well resolved. Crystal size was estimated by the well established, Williamson-Hall [22] formula applicable for adherent deposits. Microscopic studies to examine the morphology, particle size and microstructure were done by a JEOL 6480 LV scanning electron microscope (SEM) equipped with an energy dispersive X-ray detector of Oxford

data reference system. Micrographs were taken at an accelerating voltage of 5 kV for the best possible resolution from the surface rather than the interior of the deposit. Energy dispersive spectroscopy (EDS) spectra were recorded at an accelerating voltage of 20 kV and the real collection time was around 1 min. A SIEKO SPA 400 atomic force microscope (AFM) with a silicon probe was used to take the AFM figures. The micrographs presented here are in non-contact imaging mode.

3. Results and Discussion

3.1. XRD analysis

The XRD patterns of the samples synthesized at different reaction temperatures are as shown in fig.1. Decrease in either domain size or lattice strain will cause effective broadening of diffracted peaks [23]. To clearly illustrate the broadening effect, XRD patterns are represented in two parts. Fig. 1(a) shows the low angle regions of the sonicated deposits. The peak pattern shows high crystallinity of copper along with peaks from the substrate material. The diffraction peaks at $2\theta = 43.27, 50.34$ can be indexed as the (111), (200) planes of copper with cubic symmetry respectively [24]. With decreasing temperature, broadening increases where as intensity decreases. Similar XRD plateaus for decreasing crystallite size were observed by others [25,26]. Average crystallite sizes of copper deposit were determined by the Williamson-Hall formula (As Scherrer equation is valid only for powders or loosely bound deposits but not for hard and adherent deposits). The contribution of the particle size

and nonuniform strain in the grains to the observed X-ray line broadening, β, are considered to be additive generating the formula as:

$$\beta_{total} = \beta_{particle} + \beta_{strain} = \frac{(0.94\lambda)}{(t\cos\theta)} + 4\tan\theta\frac{\Delta d}{d} \quad (4)$$

The total broadening (β_{total}) is the measured FWHM in radians, corrected for instrumental broadening. The X-ray wavelength of the source Cu K_α is $\lambda = 0.15418$ nm, where t is the particle size, and 4 ($\Delta d/d$) represents the strain. Multiplying both sides of the equation by cos θ gives the final form, $\beta_{total} \cos\theta = 0.94\lambda / t + 4 \sin\theta (\Delta d/d)$, which is used to calculate the particle size and lattice strain of the copper deposit from the plot of $\beta_{total} \cos\theta$ versus sin θ. The obtained grain size variation is given in Table 1. The X-ray domains (defined as a volume that diffracts coherently) are usually much smaller than the microscopically observed grains [27].

Fig. 1(b) shows the high angle peaks of the diffraction pattern. Diffraction peaks are compared with a pure annealed copper sample. Peaks from (311) and (222) planes are present in all deposits [24]. However, the peak corresponding to the plane (400) at 2θ of 116.923 is present only in case of pure annealed copper. The above result supports the fact that diffraction from planes at high angle is not prominent with reduced grain size [23,28].

3.2. Microscopic analysis

Figs.2a-d shows the SEM morphologies of deposit at 25 ˚C, 19.5 ˚C, −1 ˚C and −3 ˚C temperatures respectively. Sonicated deposit at ambient condition shows a clear impression

of powdery morphology, while the grains are not so uniform. The grain boundaries are not so clear. Some regions are near granular, and some are highly distorted with few perforated grains. It is reasonable to assume that the distortion may be due to the ablating effect of the microstream jetting of ultrasound. The corresponding figure at silent condition is a highly branched sharp dendritic structure. At 19.5 ˚C temperature, sonicated substrate is covered by bimodal faceted copper structures as comparison to that of the truncated dendrites of the deposit without ultrasound. There are numerous big grains on the surface of copper deposits with a mean grain size of 2 μm. In addition many small grains are clearly found on these large grains. The above result may be attributed to the following factors. The surface concentration of Cu ions is high because of enhanced mass transportation by ultrasound. Hence the diffusion of Cu^{2+} improves the bulk deposition of Cu, resulting in well defined larger copper grains. The nucleation and grain growth have occurred simultaneously. Accordingly, the smaller copper grains are clearly observed on the larger grains and also on the substrate. Moreover, the result also suggests that the freshly deposited copper adatoms have moved to energy-favorable lattice sites during deposition, resulting in the distinct grain boundaries. Significant change in appearance can be observed at –1 ˚C temperature. The basic characteristic of morphology is a uniform copper covered surface with well agglomerated spheroids. The findings may reasonably be explained with the following lines. First, low temperature has resulted in high supersaturation favoring formation of smaller nuclei but in a random fashion of discharging. Second**,** ultrasound has helped in the rate of mass transportation thus creating enhanced nucleation. This effect has filled the gap between two adjacent nuclei leading to a compact mass. The above fact can be confirmed by comparing the deposit with its silent counterpart. The deposit at silent condition shows

branched structures and is not dense. Third, ultrasound helps in degassing at the electrode surface [29], leading to an adherent and bright deposit [16]. The deposit at –3 ˚C shows uniform and fully coalesced fine grained copper coating on graphite with ultrasound. A comparison with the counterpart silent deposit, confirms the fact mentioned above.

A comparative compositional analysis from the EDS result has given in Table 2. The results shows that with decreasing temperature the impurity levels mainly at% of oxygen is increasing in silent deposit where as sonication depositions have zero levels of contamination. Oxygen content has got increased roughly with decreased temperature. EDS plot of the above mentioned fact has been given in fig. 3. Compound analysis from the Oxford data shows that the oxides at high temperatures are mainly CuO and Cu_2O at low temperatures. The fact that ionic character tends to increase [30] with reducing grain size and high symmetry structures are stable at low temperatures [31] might have resulted the above compositional variation in silent conditions. Sulfur content of the deposit also shows a decreasing trend with temperature. The element usually gets adsorbed on the substrate from the electrolyte. Low temperature has reduced the adsorption tendency of the same. Due to the presence of a highly dynamic energy system, the conditions for the formation of the above weak covalent bond between copper and oxygen might have not been possible in ultrasonic field. Unlike the deposit in silent condition, the deposit obtained is free from adsorbed sulfur due to in-situ cavitational cleaning of the electrodes.

Height mode topographical AFM micrographs of the deposits at –1 ˚C and –3 ˚C temperatures are shown in fig.4. The deposits at –1 ˚C are copper spheroids of average height and size of 30-40 nm and the surface is nearly uniform as confirmed by the phase image of the deposit. Whereas the deposits at –3 ˚C show an average height of around 172 nm in

contrast to the XRD domain size of 6 nm. The above discrepancy of the two methods is solved by a meticulous topographical analysis of the cluster and inter-cluster topographical height images. For the samples prepared at –3 °C, the clusters have grains in the size range of 20-30 nm. The high surface energy associated with the decreased size might have caused the deposits to agglomerate to a great extent.

3. Conclusion

An attempt has been made to explore the use of low temperature electrochemistry in synthesizing nanoparticles in ultrasound cavitation condition. The crystallinity and morphology of the deposits have been characterized by XRD, SEM and AFM. In spite of the complicated and wide variation of morphologies and microstructures, the fact that thedeposits belong to the nano range has been confirmed. A thorough compositional analysis of the deposits by EDS shows a cleaner sonicated deposit as compared to a highly oxidized silent deposit, which contains traces of adsorbed sulfur. The present investigation is further directed to explore the possibility of making nano sized particles at further sub-ambient temperatures. Statistically significant data are needed, to evaluate the science of synergistic effects of sonication and temperature during electrochemical synthesis. The exploration of this technique needs wider investigation and critical assessment before drawing a conclusion.

Acknowledgement

The authors would like to thank the National Institute of Technology (NIT) for providing the necessary financial support. Authors are also grateful to National Metallurgical Laboratory, Jamshedpur for the infrastructure support.

Reference

[1] D. Floner, F. Geneste, Electrochem. Commun. 9 (2007) 2271.

[2] O. Ghodbane, L. Roue, D. Belanger, Electrochim. Acta 52 (2007) 5843.

[3] C. C. Hu, C. M. Wu, Surf. Coat. Technol. 176 (2003) 75.

[4] G. Gunawardena, G. Hills, I. Montenegro, B. Scharifker, J. Electroanal. Chem. 138 (1982) 225.

[5] G. Staikov, A. Milchev, in: G. Staikov (Ed.), Electrocrystallization in Nanotechnology, Wiley VCH, Weinheim, 2007, p.1.

[6] I. V. Morkov, Crystal Growth for Beginners, World Scientific, Singapore, 1995.

[7] J. H. Perpezko, in: D. M. Stefenescu, Metals Handbook, Vol. 15, ASTM International, Ohio, 1988, p. 99.

[8] L. Zhang, Z. Chen, Y. Tang, Z. Jia, Thin Solid Films 492 (2005) 24.

[9] E. W. Bohannan, C. C. Jaynes, M. G. Shumsky, J. K. Barton, J. A. Switzer, Solid State Ionics 131 (2000) 97.

[10] J. P. Lorimer, T. J. Mason, Applied Sonochemistry: Uses of power ultrasound in chemistry and Processing, Wiley VCH, Weinheim, 2002.

[11] A. R. Naji Meidani, M. Hasan, Appl. Math. Model. 28 (2004) 333.

[12] S. Devarakonda, J. M. B. Evans, S. Myerson, Cryst. Growth Des. 3 (2003) 741.

[13] C. A. G. Leyva, A. Q. Ramos, J. Barnard, R. R. B. Quintana, R. T. Abbud, J. J. Castro, J. Food Eng. 81 (2007) 374.

[14] F. J. D. Campo, A. Neudeck, R. G. Compton, F. Marken, J. Electroanal. Chem. 477 (1999) 71.

[15] C. A. Gutierrez, J. L. Hardcastle, J. C. Ball, R. G. Compton, The Analyst 124 (1999) 1053.

[16] E. Namgoong, J. S. Chun, Thin Solid Films 120 (1984) 153.

[17] T. J. Mason, J. P. Lorimer, S. Saleem, I. Paniwnyk, Environ. Sci. Technol. 35 (2001) 3375.

[18] X. Chai, T. Kobayashi , N. Fujii, Sep. Purif. Technol. 15 (1999) 139.

[19] C. E. Banks, R. G. Compton, Electroanalysis 15 (2003) 329.

[20] M. E. Hyde, R. G. Compton, J. Electroanal. Chem. 531 (2002) 19.

[21] C. E. Banks, R. G. Compton, A. C. Fischer, I. E. Hanley, Phys. Chem. Phys. Chem. 6 (2004) 3147.

[22] G. K. Williamson, W. H. Hall, Acta Metall. 1 (1953) 22.

[23] B. D. Cullity, Elements of X-Ray Diffraction, Addison-Wesley Publisher, MA, 1978.

[24] International Centre for Diffraction Data (ICDD), Card No. 04-0863.

[25] R. P. Raffaelle, T. Potdevin, A. F. Hepp, S. G. Bailey, Mater. Sci. Semicond. Process. 2 (1999) 289.

[26] M. H. Seo, D. J. Kim, J. S. Kim, Thin Solid Films 489 (2005) 122.

[27] H. M. Xu, H. G. Yan, Z. H. Chen, Mater. Charact. 59 (2008) 301.

[28] C. Suryanarayan, M. Grant Norton, X-ray Diffraction a Practical Approach, Plenum Press, NY, 1998.

[29] H. Yanagida, Ultrason. Sonochem. 15 (2008) 492.

[30] H. Yanagimoto, K. Akamatsu, K. Gotohb, S. Deki, J. Mater. Chem. 11 (2001) 2387.

[31] V. R. Palkar, P. Ayyub, S. Chattopadhyay, M. Multani, Phys. Rev. B 53 (1996) 2167.

FIGURE CAPTIONS

Figure 1. XRD patterns of copper films prepared by sonication at different temperature at low and high 2θ values

Figure 2. SEM images of copper deposits with and without sonication at 25, 19.5, –1 and –3 ˚C.

Figure 3 EDS spectra of copper deposits prepared at 25 ˚C

(a) Without sonication

(b) With sonication

Figure 4. AFM images of copper deposits prepared with sonication at

(a) −1 ˚C

(b) −3 ˚C

Table 1 XRD grain size and lattice strain of sonicated copper deposits

Temperature in ˚C	Grain Size in nm	Lattice Strain
25	210	0.005
19.5	28	0.021
–1	22	0.024
–3	6	0.070

Table 2 Composition of copper deposits deposited with and without sonication as measured by EDS

Temperature	Silent Composition (at%)			Sonication Composition (at%)		
	Cu	O	S	Cu	O	S
25	76	21	3	100	-	-
19.5	72	26	2	100	-	-
–1	65	34	1	100	-	-
–3	62	37	1	100	-	-

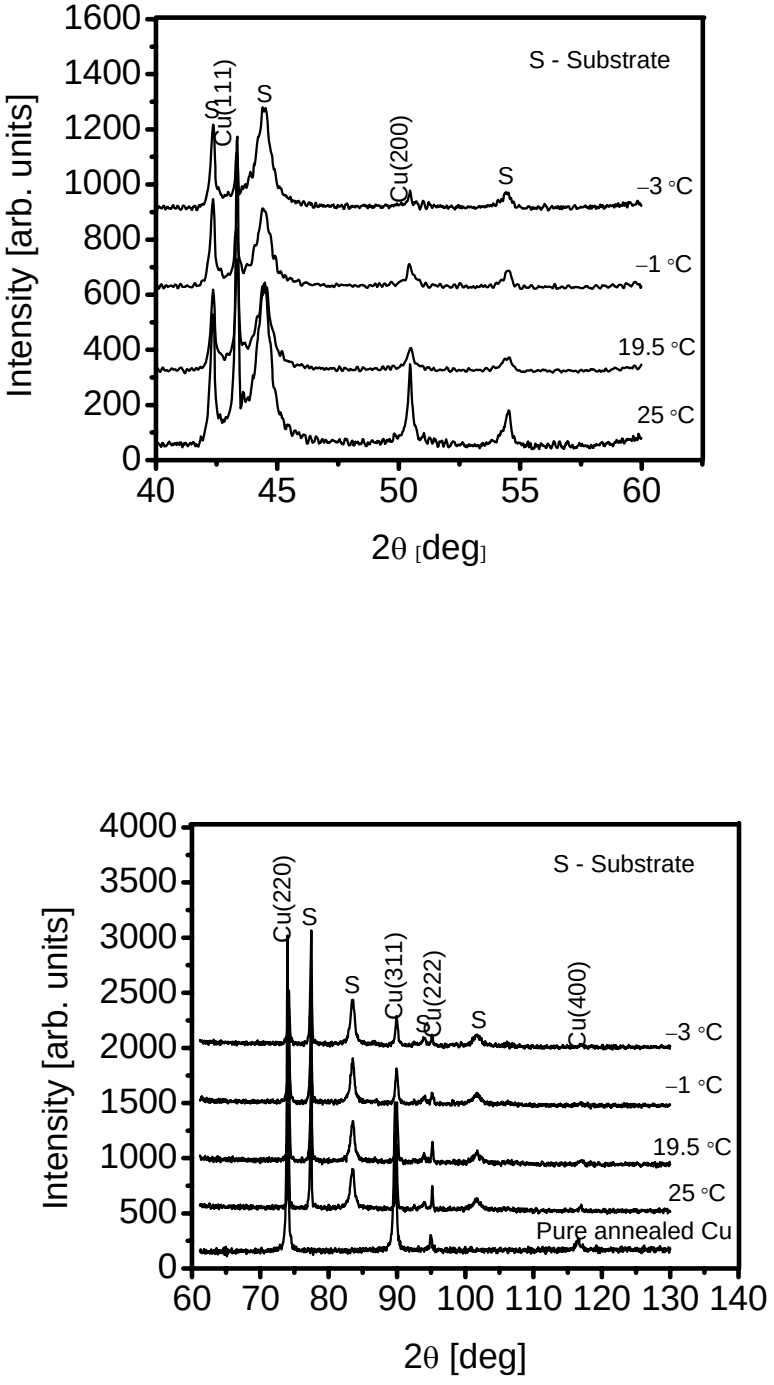
S - Substrate
Cu(111)
S
Cu(200)
S
–3 °C
–1 °C
19.5 °C
25 °C
Intensity [arb. units]
2θ [deg]
S - Substrate
Cu(220)
S
S
Cu(311)
Cu(222)
S
Cu(400)
–3 °C
–1 °C
19.5 °C
25 °C
Pure annealed Cu
Intensity [arb. units]
2θ [deg]

Figure 1

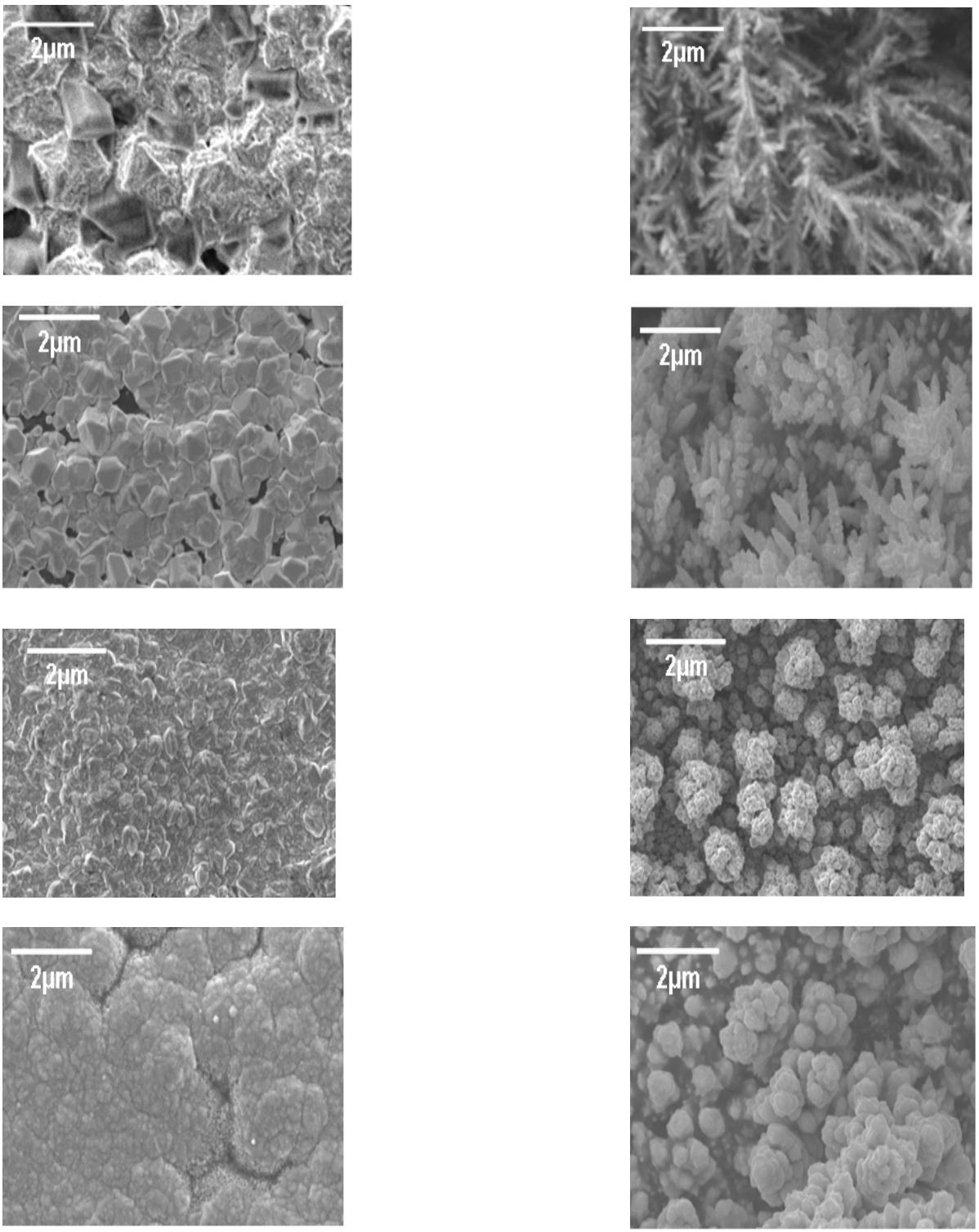

Figure 2

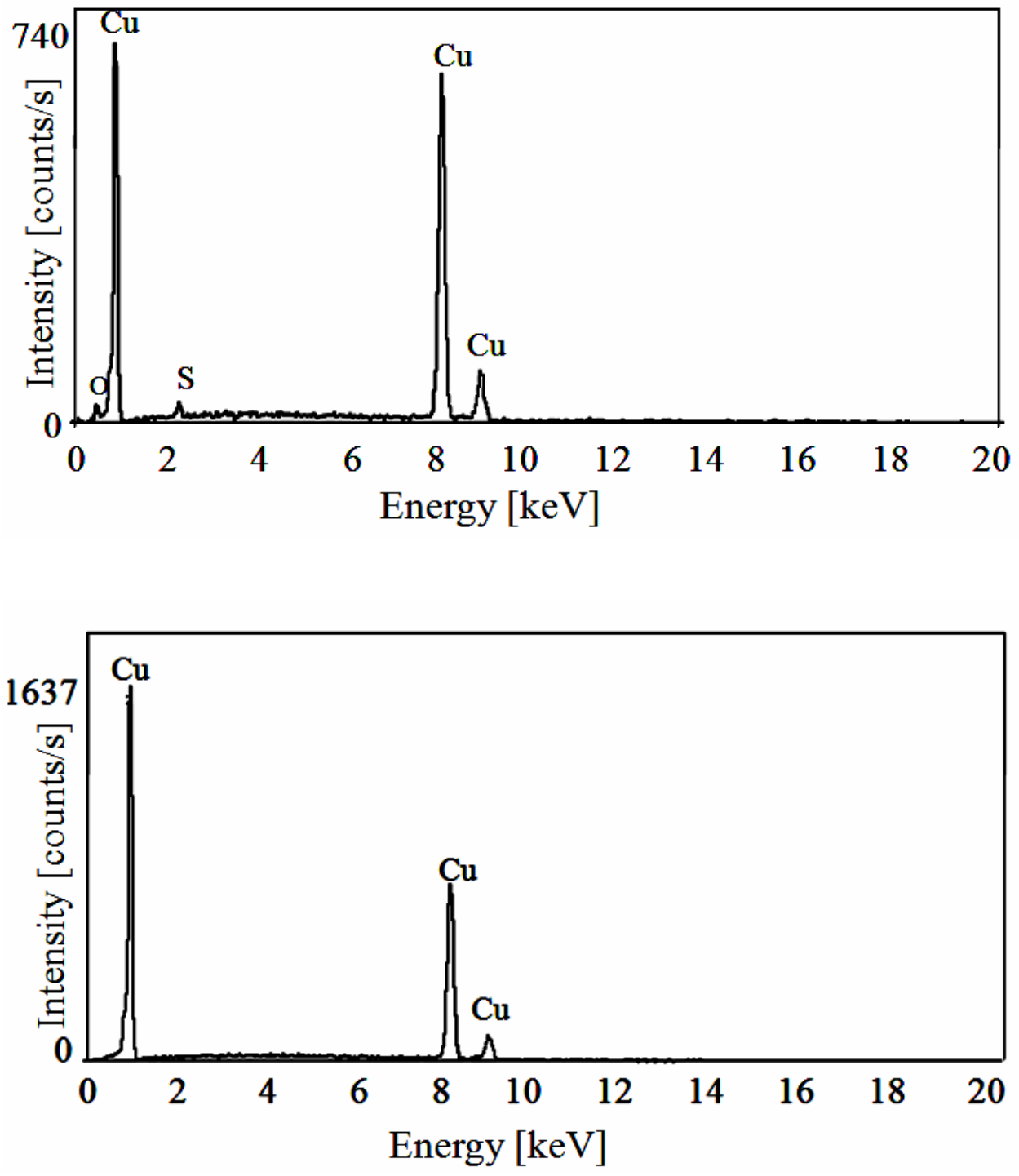
740
Cu
Cu
Cu
O
S
Intensity [counts/s]
0
0 2 4 6 8 10 12 14 16 18 20
Energy [keV]
1637
Cu
Cu
Cu
Intensity [counts/s]
0
0 2 4 6 8 10 12 14 16 18 20
Energy [keV]

Figure 3

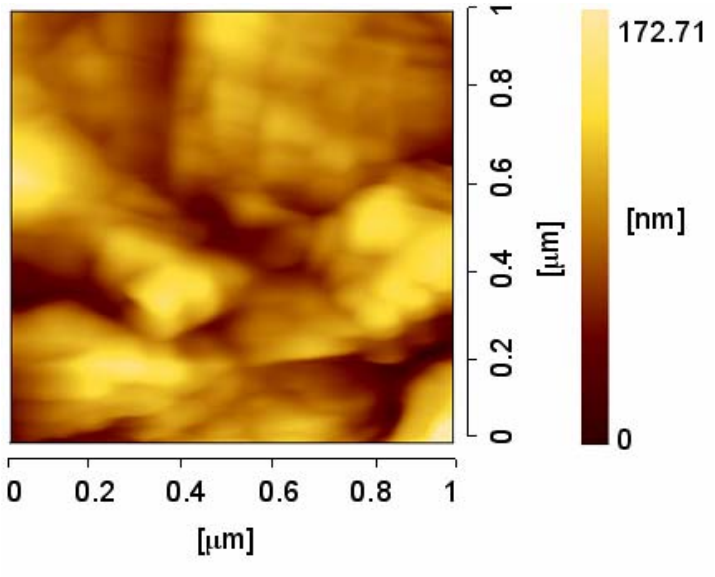
172.71
[nm]
0
[µm]
0
0.2
0.4
0.6
0.8
1
0
0.2
0.4
0.6
0.8
1
[µm]

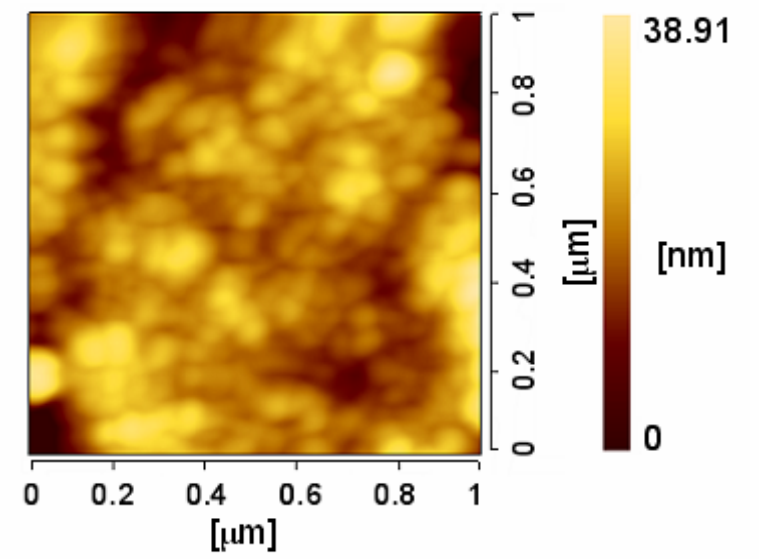
38.91
[nm]
0
[µm]
0
0.2
0.4
0.6
0.8
1
0
0.2
0.4
0.6
0.8
1
[µm]